Journal of
Materials in Life Sciences

Vol. 4 No. 1 (2025)

Full Paper

In Silico RNA Aptamer Targeting the Receptor Binding Domain of the SARS-CoV-2 Omicron Variant Spike Protein

Khavithra Gobala Krisnan, Anas Al-obaidi, Huszalina Hussin, Razauden Mohamed Zulkifli*

Department of Biosciences, Faculty of Science, Universiti Teknologi Malaysia, 81310 UTM Johor Bahru, Johor, Malaysia.

Article history
Received
22 May 2025
Revised
25 May 2025
Accepted
27 May 2025
Published online
31 May 2025

*Corresponding author
razauden@fbb.utm.my

Abstract

The COVID-19 pandemic, caused by the SARS-CoV-2 virus, remains a global health challenge, particularly with the emergence of highly mutated variants like Omicron. The receptor binding domain (RBD) of the spike protein is essential for viral entry into host cells, making it a crucial target for diagnostics and therapeutics. Aptamers are short, single-stranded oligonucleotides that have gained attention as promising molecular recognition elements due to their strong binding affinity and specificity for viral proteins. This study aims to develop an RNA aptamer targeting the Omicron RBD. Initially, an oligonucleotide pool was constructed using RANDNA software and evaluated based on secondary structure properties. The 3D structures of the filtered sequences were modelled and docked with the Omicron RBD to identify the best aptamer candidates. The top three aptamer candidates exhibited the highest number of binding site interactions and were chosen for further analysis using molecular dynamics simulations. APT 6 exhibited a negative docking score (-19.2 kcal/mol) and formed the greatest number of interactions with the mutated amino acids (G446S, Q493R, G496S, Q498R, N501Y and N505H) within the binding site. The RMSD and RMSF analyses of the complex indicate good stability and flexibility, while Rg measurements reflected a compact and stable structure. The findings suggest that APT 6 is tailored for detecting the Omicron variant, indicating its potential utility as a diagnostic tool.

Keywords COVID-19, Omicron, *in silico*, aptamer, molecular docking, molecular dynamics simulations

1.0 INTRODUCTION

Coronavirus disease 2019 (COVID-19), caused by severe acute respiratory syndrome coronavirus 2 (SARS-CoV-2), has led to millions of deaths worldwide [1]. The virus' genome consists of single-stranded RNA and encodes structural proteins, which are spike (S), envelope (E), membrane (M), and nucleocapsid (N), along with 16 non-structural proteins [2]. The S protein is crucial for viral entry, binding to the host angiotensin-converting enzyme (ACE2) receptor via its S1 subunit and facilitating membrane fusion through the S2 subunit. Given its role in infectivity, the S protein is a primary target for diagnostics, vaccines, and therapeutics [3].

The Omicron variant, with 60 mutations, exhibits enhanced transmissibility and immune resistance, particularly due to changes in its receptor binding domain (RBD) [4]. Some key mutations such as K417N, E484A, and N501Y increase binding affinity to ACE2, contributing to its high infectivity [5]. The RBD is central to vaccine development and diagnostics, as neutralizing antibodies target it to prevent viral entry [6].

Precise and early identification of SARS-CoV-2 enables the rapid isolation of infected individuals, reducing the risk of virus transmission within communities. A polymerase chain reaction (PCR) based assay is regarded as the gold standard for the detection of viruses because of its sensitivity and specificity [7]. However, there are many limitations to RT-PCR-based techniques, including the need for a highly pure sample, expensive laboratory equipment, specialist training, and a long reaction time [8]. Besides, COVID-19 antigen rapid test kits, developed using lateral flow immunoassay technology, can quantitatively detect the SARS-CoV-2 antigen. These tests have a sensitivity of approximately 85% [9].

Aptamers, short single-stranded nucleic acids, offer an alternative to antibodies for viral detection due to their high specificity, stability, and ease of synthesis [10]. The Systematic Evolution of Ligands by Exponential Enrichment (SELEX) technique is commonly used to develop aptamers, but it can be labour-intensive and non-specific binding [11]. Computational approaches have emerged to address these challenges, allowing for the *in silico* design and evaluation of an RNA aptamer specifically targeting the RBD of the SARS-CoV-2 Omicron variant S protein.5Molecular dynamics (MD) simulations provide further insights into binding interactions, enhancing our understanding of the aptamer-protein complexes.

2.0 METHODOLOGY

2.1 Data collection

RANDNA software (http://www.introni.it/software.html) was used to generate a pool of 60000 random RNA aptamers, each 30 nucleotides long, ensuring equal representation of adenine (A), cytosine (C), guanine (G), and uracil (U) at 25% each. RANDNA enhances computational aptamer analysis through robust simulation and user-friendly design. Additionally, the RBD structure of the SARS-CoV-2 Omicron variant S protein (PDB ID: 7QNW) [12] was retrieved from the Protein Data Bank (https://www.rcsb.org/) for further study.

2.2 Prediction of 2D structure and sorting of RNA sequences

The library of 60000 random RNA sequences was imported into RNAFold web server (https://www.unafold.org/mfold/applications/rna-folding-form.php) using default parameters to ensure consistency. The output file included sequence details such as predicted secondary structure, free energy (ΔG), enthalpy (ΔH), entropy (ΔS), and melting point (Tm). Predominantly, simple hairpin structures were observed. Sequences with ΔG lower than -16.0 were filtered for stability under physiological conditions, reducing the pool from 60000 to 6 for further analyses.

2.3 Prediction of the 3D structure of the selected RNA sequences

The 3D structure of the selected RNA sequences was predicted using RNA composer online server (https://rnacomposer.cs.put.poznan.pl/). This was achieved by using dot-bracket notation Vienna File, which was previously downloaded from RNAFold web server. This software was chosen because it is a user-friendly interface that allows for automatic high-quality predictions of the 3D structure.

2.4 Energy minimization of protein structure and selected RNA sequences

Non-protein components were removed from the protein structure using Biovia Discovery Studio, followed by energy minimization in Swiss PDB Viewer with the GROMACS 43B1 forcefield [13]. For aptamer sequences, UCSF Chimera was used with the AMBERffsb forcefield, ensuring compatibility with downstream docking studies [14].

2.5 Preparation of protein and selected RNA sequences

The energy-minimized protein was selected for the docking process. Before docking studies, the protein structure was checked for missing atoms and repaired. The addition of polar hydrogen atoms and Kollmann charges was performed using Autodock Vina. The protein structure was saved as PDBQT extension. Next, the preparation of the selected RNA sequences. The PDB format files of these sequences were changed to PDBQT format by using the Openbabel GUI. After the conversion, these sequences were uploaded and prepared using Autodock Vina.

2.6 Molecular Docking

The docking process was carried out by setting the protein's binding site with a grid box centered at x = -15.933, y = 15.814, and z = -23.667, with dimensions of 100 X 100 X 90 Å, covering 22 binding site residues (K417N, G446S, Y449, Y453, L455, F456, Y473, A475, G476, S477N, E484A, F486, N487, Y489, F490, Q493R, G496S, Q498R, T500, N501Y, G502 and N505H) [15]. Based on known binding site residues, the dimensions of the grid box were determined. Having a well-defined grid box ensures optimal coverage for docking simulations and eventually allows accurate docking. Furthermore, the exhaustiveness of the Autodock Vina 4.2 was set to 16. In the docking process, the exhaustiveness determines how many independent runs to perform. This optimization enhances the identification of binding modes and increases scoring accuracy [16]. All the screened RNA sequences were docked with Omicron RBD (7QNW) to obtain the best aptamer candidates.

2.7 Molecular Dynamics Simulations

MD simulations were conducted for the top three Omicron RBD-aptamer complexes, which exhibited the highest number of interacting binding site residues during molecular docking, irrespective of their docking score. Each receptor-ligand complex

was uploaded in CHARMM-GUI Membrane Builder, an online platform for constructing protein membrane systems and preparing inputs for MDS [17]. For the water box size, the option to automatically adjust the dimensions to fit the complex was selected, and the transferable intermolecular potential with the 3 points (TIP3P) water model was automatically chosen by this membrane builder. The Monte Carlo ion placing method was employed to equalize the system by adding enough K^+ and Cl^- ions, followed by setting its salt concentration to 0.15 M. Next, during the setup of periodic boundary conditions, the option labelled as "Generate grid information for PME FFT automatically" was selected. Finally, the CHARMM36m force field was selected for the simulation, the input generation option was set to GROMACS, and the temperature was fixed at 310.15 K using a two-step ensemble process (NVT and NPT) [17]. Upon completion of the system preparation, the system underwent MDS for 50ns. Previous studies frequently used similar simulation durations for comparable systems [18]. Following the MD simulation, the conformational changes in the Omicron RBD-Aptamer complex over time were visualized using Visual Molecular Dynamics (VMD). Analysis of all trajectory files was performed with the GROMACS package, considering root mean square deviation (RMSD), root mean square fluctuation (RMSF), radius of gyration (Rg), and hydrogen bonding.

3.0 RESULTS AND DISCUSSION

3.1 RNA Sequence Generation and Secondary Structure Prediction

This study employed RANDNA software to generate a comprehensive library of 60000 RNA sequences, each 30 nucleotides in length. With the help of RNAFold software, six sequences were selected using filtration criteria and denoted as APT 1, APT 2, APT 3, APT 4, APT 5, and APT 6 for easier identification. Structures exhibiting loops, bulges, and stems with lower minimum free energy (ΔG) were prioritized for their predicted stability and potential functional importance. Key parameters ΔG, ΔH, ΔS, and Tm were derived (Table 1), supporting the structural evaluation. 2D structures were further processed into 3D models (Figure 1) using RNA Composer. Energy minimization of Omicron RBD and aptamer models was performed using Swiss PDB Viewer and UCSF Chimera, respectively. Unnecessary chains and non-protein components were removed from the receptor, as their presence can interfere with docking accuracy [19].

Table 1 Selected aptamers and their parameters predicted using the RNAFold web server

Aptamer	Sequence	ΔG (kcal/mol)	ΔH (kcal/mol)	ΔS (kcal/kmol)	Melting point (Tm)
APT 1	GGCGGCGGAGGGUAAGGCCUCCCUGCCAAC	-16.60	-113.60	-312.75	90.1
APT 2	GACUAACUAGUCGCAAGACUAGUUAGUGCA	-17.10	-108.00	-293.08	95.4
APT 3	CGCGGCUUCGGCCGCUUGGGACUCUGUCCC	-17.80	-115.40	-314.69	93.6
APT 4	GAGAGACACCGAGCGGCAACGCUGGUGUCU	-17.70	-114.70	-312.75	93.6
APT 5	GGCAUGGGCCUACCAGAGGCUCGUGCAAGC	-17.80	-100.40	-266.32	103.8
APT 6	GGAUGGGCGCCGGCUUACUCGCGCUCAUCG	-16.10	-112.40	-310.49	88.9

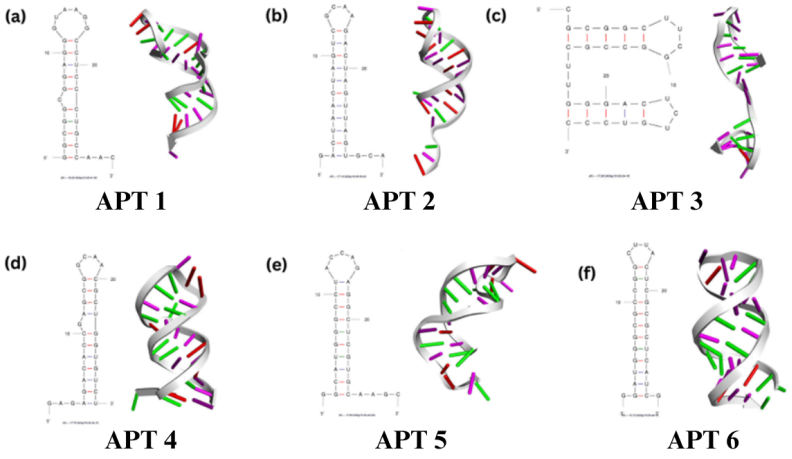

Figure 1 The 2D and 3D structures of aptamers

3.2 Molecular Docking

Molecular docking was performed on six aptamer candidates to evaluate their binding affinities and interactions with the Omicron RBD. Docking scores (Table 2) ranked APT 6 as the best, followed by APT 3 and APT 2. Interaction profiles and 2D/3D structures revealed the extent of binding site interactions. Docking scores ranged from -16.9 to -19.2 kcal/mol, with APT 6 showing the best binding affinity at -19.2 kcal/mol, indicating its strong interaction with the Omicron RBD. APT 6 (Figure 7) interacted with 16 of the 22 binding site residues, including six mutated residues (G446S, Q493R, G496S, Q498R, N501Y, and N505h), enhancing its binding and stability. APT 3 (Figure 4), despite a good docking score, did not interact with the binding site residues, highlighting the importance of actual interactions for effective binding APT 2 (Figure 3) had only one binding site interaction, suggesting weaker binding affinity.

Table 2 Omicron RBD-Aptamer complexes and its docking score

Omicron RBD-Aptamer complex	Docking score (kcal/mol)
Omicron RBD-APT 1	-17.3
Omicron RBD-APT 2	-18.3
Omicron RBD-APT 3	-18.4
Omicron RBD-APT 4	-18.2
Omicron RBD-APT 5	-16.9
Omicron RBD-APT 6	-19.2

APT 4 (Figure 5) showed strong interaction with 12 binding site residues, including four mutated residues (K417N, Q498R, N501Y, and N505H), enhancing its binding affinity. APT 1 (Figure 2) formed 11 interactions with three mutated residues (K417N, Q493R, and N505H), contributing to its stability and binding affinity. APT 5 (Figure 6) had only one interaction, indicating lower binding affinity. The top three candidates, APT 1, APT 4, and APT 6, which formed maximum number of interactions with the Omicron RBD, were selected for further analysis through MD simulations (Table 3).

Table 2 Selected complexes and their interactions with maximum binding site residues (**Bolded in black**)

Omicron RBD-Aptamer complexes (interaction with maximum binding site residues)	Interactions	Residues
Omicron RBD-APT 1	Conventional hydrogen bond	TYR 421 **TYR 489-2** **ARG 493** **ASN 487**
	Carbon hydrogen bond	**ASN 417**
	Van der Waals	ARG 403 THR 415 GLY 416 **TYR 453** **LEU 455** **PHE 456** ASN 460 **TYR 473** **ALA 475** **PHE 486** **HIS 505**
	Unfavourable bond	**ASN 417** ASP 420
Omicron RBD-APT 4	Salt bridge	ARG 403-2
	Attractive Charge	ARG 403-2 ARG 408 LYS 458

	Conventional hydrogen bond	GLN 409-2 **ASN 417-3** TYR 421 **ALA 475** **ARG 498** GLY 504
	Carbon hydrogen bond	GLY 416 GLY 504 GLU 406 LYS 458 **HIS505**
	Van der Waals	ASP 405 THR 415 ILE 418 **TYR 453** **LEU 455** **PHE 456** ARG 457 SER 459 ASN 460 **TYR 473** **GLY 476** **TYR 489** **TYR 501** **GLY 502** VAL 503
	Pi-Anion	**HIS 505**
	Unfavourable bond	GLN 409
Omicron RBD-APT 6	Salt bridge	**ARG 493-2**
	Attractive charge	LYS 478
	Conventional hydrogen bond	**SER 446** **ARG 498** **THR 500**
	Carbon hydrogen bond	**SER 496**
	Van der Waals	ASP 405 THR 415 ILE 418 **TYR 453** **LEU 455** **PHE 456** ARG 457 SER 459 ASN 460 **TYR 473** **GLY 476** **TYR 489** **TYR 501** **GLY 502** VAL 503
	Pi-Anion	**PHE 490** **TYR 449**
	Pi-Pi Stacked Pi-Pi T-shaped	**HIS 505-2** **TYR 501**

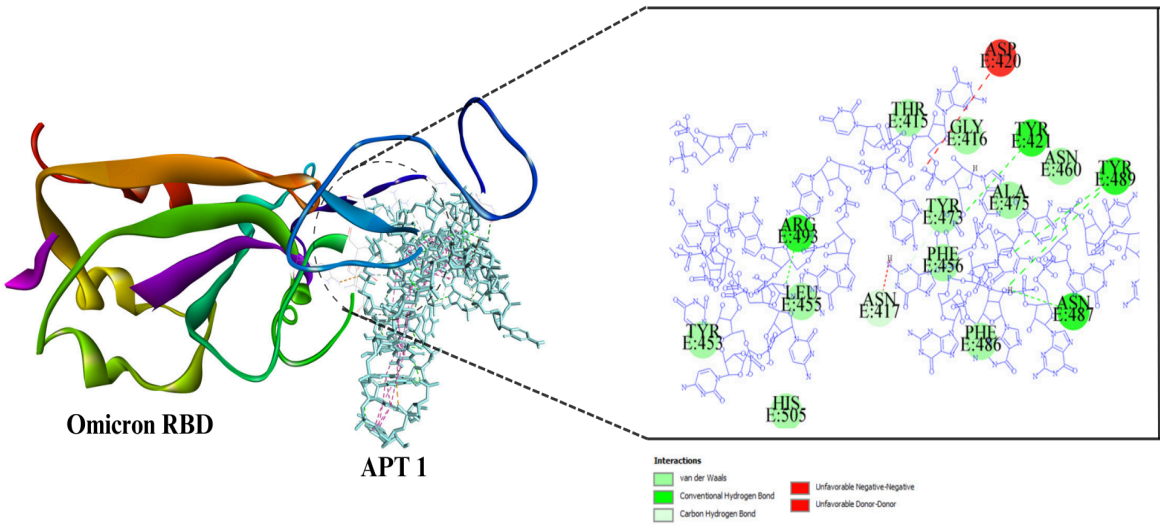

Figure 2 Docking analysis of Omicron RBD-APT 1. The APT 1 docked with Omicron RBD, and the interaction between the APT 1 and Omicron RBD was visualized by Biovia Discovery Studio. Several crucial interactions were formed between the complex, such as hydrogen bonds and van der Waals, which indicate stable binding of the APT 1 to the Omicron RBD.

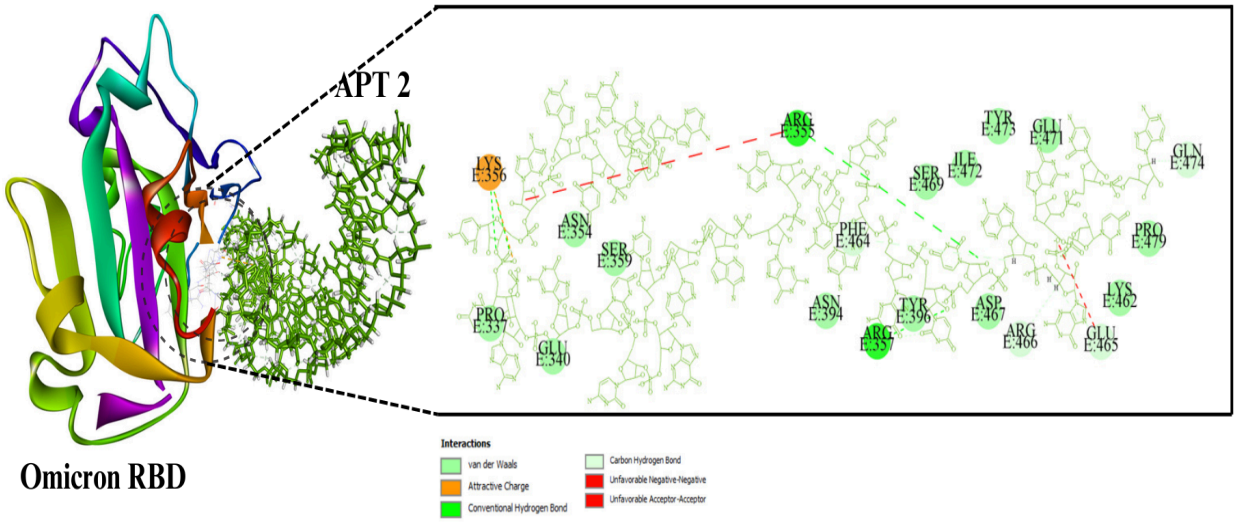

Figure 3 Docking analysis of Omicron RBD-APT 2. The APT 2 docked with Omicron RBD, and the interaction between the APT 2 and Omicron RBD was visualized by Biovia Discovery Studio. Several crucial interactions were formed between the complex, such as hydrogen bonds, attractive charges, and van der Waals, which indicate stable binding of the APT 2 to the Omicron RBD.

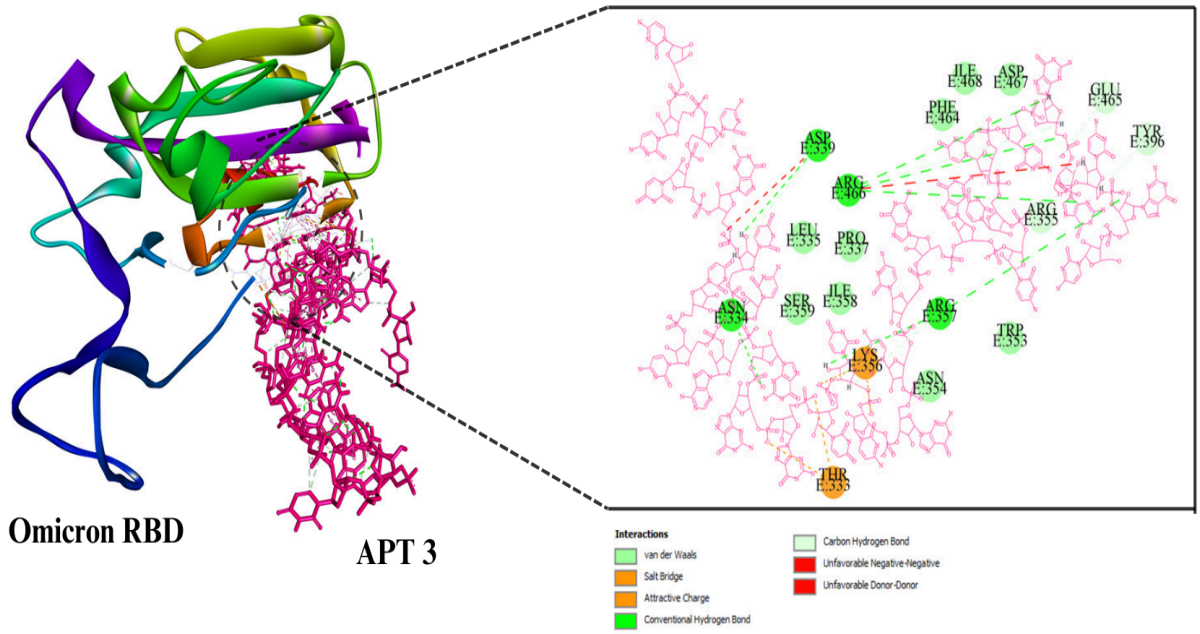

Figure 4 Docking analysis of Omicron RBD-APT 3. The APT 3 docked with Omicron RBD, and the interaction between the APT 3 and Omicron RBD was visualized by Biovia Discovery Studio. Several crucial interactions were formed between the complex, such as hydrogen bonds, salt bridge, attractive charges, and van der Waals, which indicate stable binding of the APT 3 to the Omicron RBD.

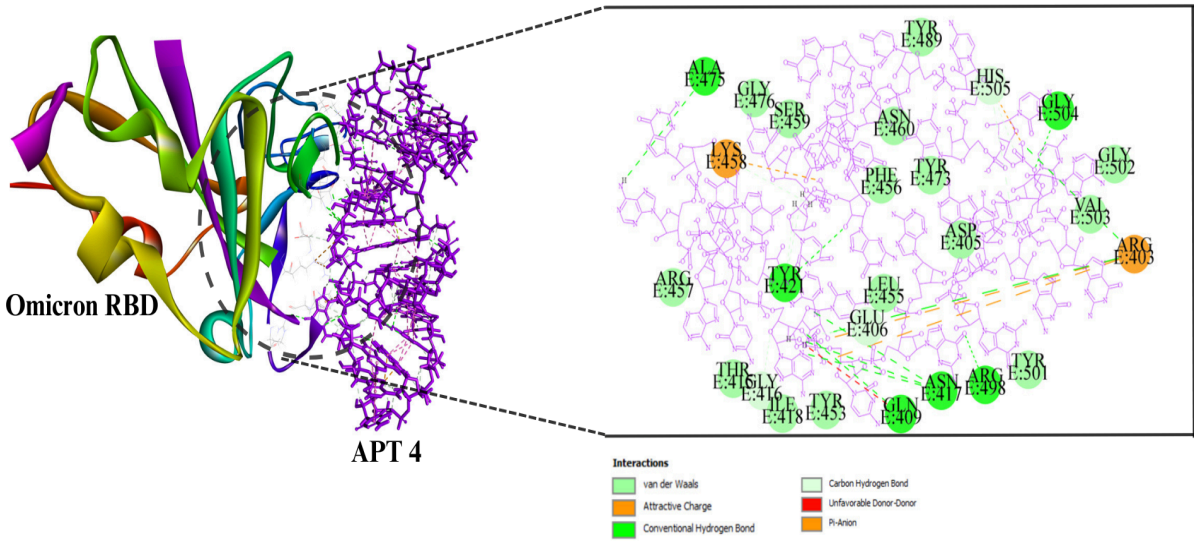

Figure 5 Docking analysis of Omicron RBD-APT 4. The APT 4 docked with Omicron RBD, and the interaction between the APT 4 and Omicron RBD was visualized by Biovia Discovery Studio. Several crucial interactions were formed between the complex, such as hydrogen bonds, attractive charges, and van der Waals forces, which indicate stable binding of the APT 4 to the Omicron RBD.

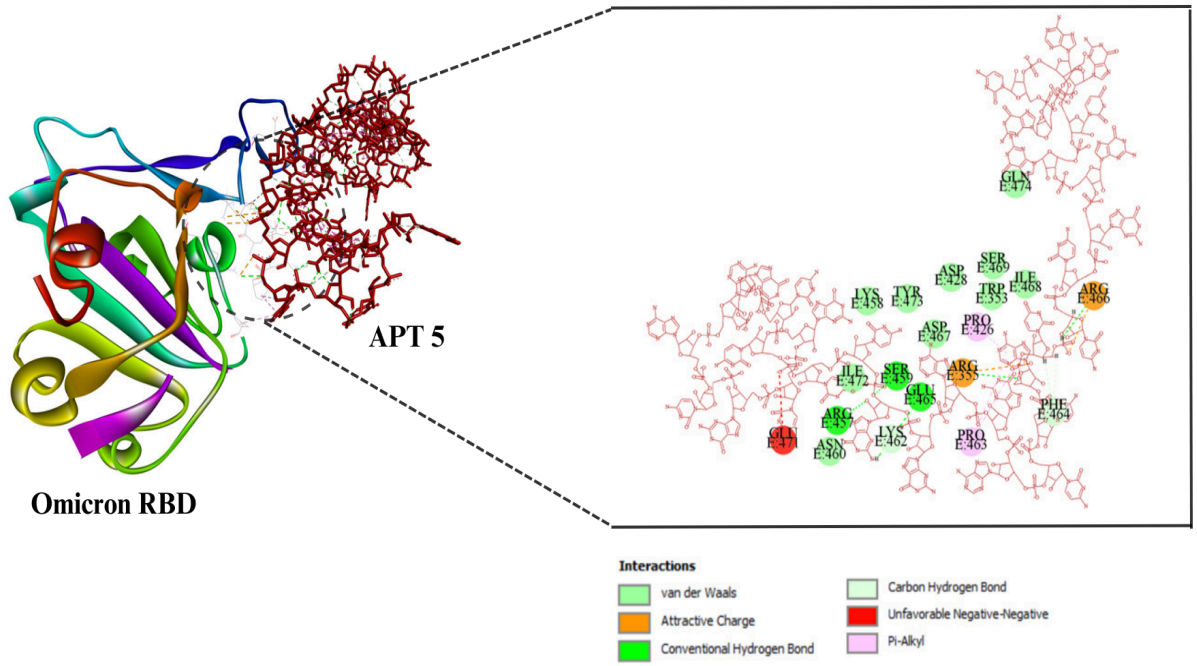

Figure 6 Docking analysis of Omicron RBD-APT 5. The APT 5 docked with Omicron RBD, and the interaction between the APT 5 and Omicron RBD was visualized by Biovia Discovery Studio. Several crucial interactions were formed between the complex, such as hydrogen bonds, attractive charges, and van der Waals, which indicate stable binding of the APT 5 to the Omicron RBD

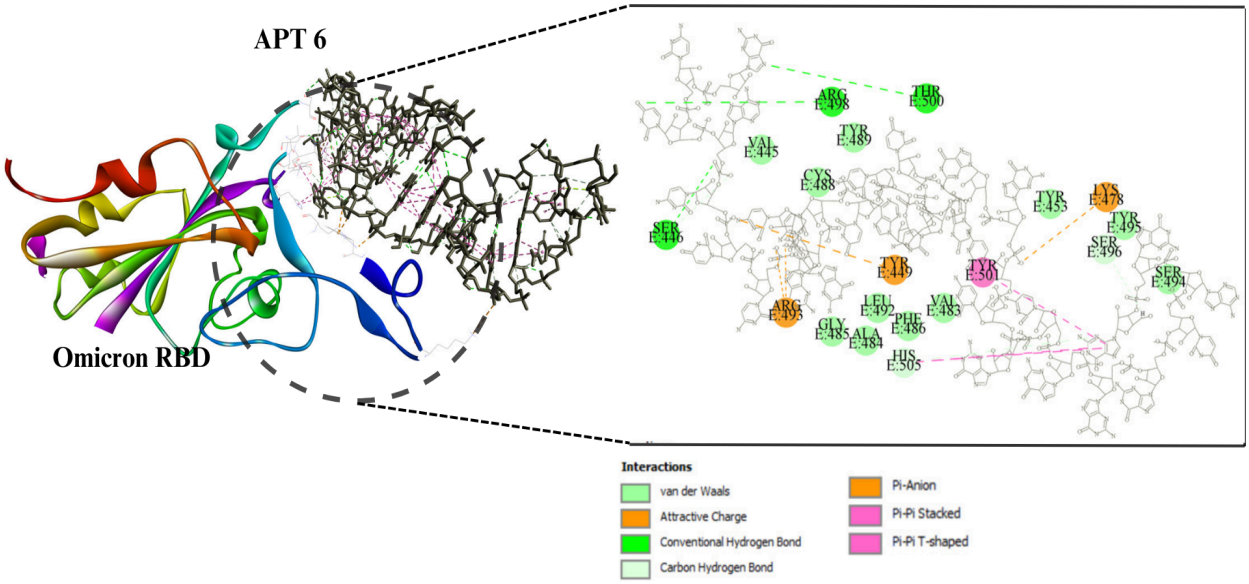

Figure 7 Docking analysis of Omicron RBD-APT 6. The APT 6 docked with Omicron RBD, and the interaction between the APT 6 and Omicron RBD was visualized by Biovia Discovery Studio. Several crucial interactions were formed between the complex, such as hydrogen bonds, attractive charges, and van der Waals, which indicate stable binding of the APT 6 to the Omicron RBD.

3.3 Molecular dynamics simulations analysis

RMSD plays a crucial role in evaluating structural stability and allows comparative analysis of molecular conformations at an atomic level [20]. In this study, the Omicron RBD showed a steady state RMSD throughout the simulation run with a low fluctuation of about 0.2 Å (Figure 8a). This signifies a robustly stable conformation with negligible structural deviation,

indicating that the RBD preserves its native fold throughout the simulation. The RMSD of Omicron RBD-APT 1 rose to 1.5 Å at 15400 ps and then remained stable between 1.2 Å and 1.7 Å until the end of the simulation (Figure 8a). This gradual rise, followed by stabilization, indicates that the complex undergoes initial conformational shifts before attaining equilibrium, preserving its structural integrity throughout. The RMSD of Omicron RBD-APT 4 complex rose to 2.3 Å at 6200 ps and then remained stable between 1.9 Å and 2.6 Å until the end of the simulation. The elevated RMSD values relative to the other complexes suggest increased conformational flexibility or structural rearrangement upon binding with APT 4. However, the plateau phase signifies that the complex ultimately reaches a stable conformation throughout the simulation. The RMSD of Omicron RBD-APT 6 complex rose to 1.5 Å at 3100 ps and then remained stable between 0.7 Å and 1.2 Å until the end of the simulation. This trend indicates an initial structural adaptation, followed by a stable binding conformation with fewer fluctuations than the Omicron RBD-APT 4 complex. Overall, all complexes achieve equilibrium and maintain stability beyond 35ns of simulation time.

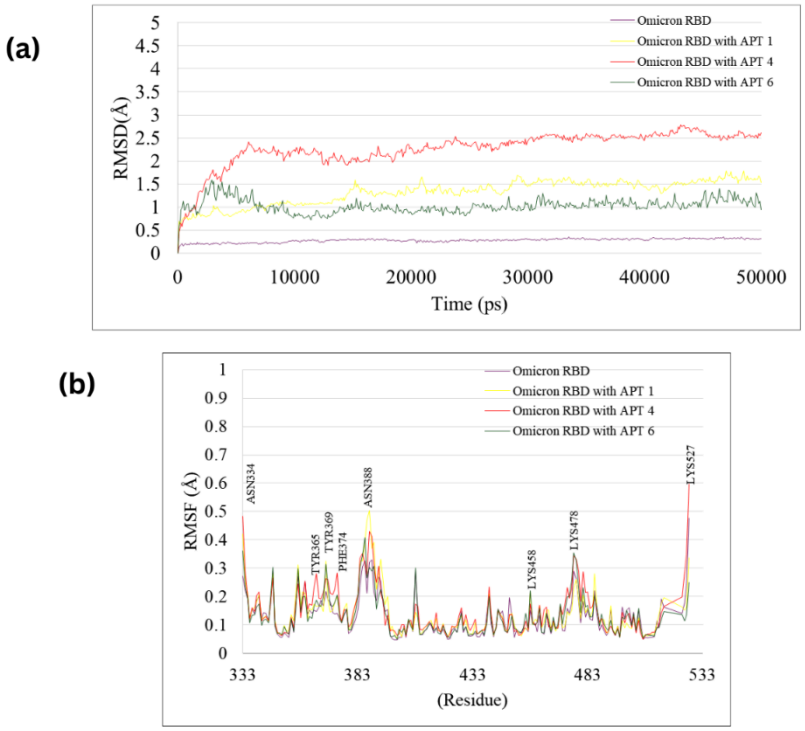

Figure 8 The RMSD and RMSF of Omicron RBD and Omicron RBD-Aptamer complexes. (a) RMSD of [Omicron RBD (purple), Omicron RBD-APT 1 (yellow), Omicron RBD-APT 4(red), and Omicron RBD-APT6 (green)]. (b) RMSF of [Omicron RBD (purple), Omicron RBD-APT 1 (yellow), Omicron RBD-APT 4(red), and Omicron RBD-APT6 (green)].

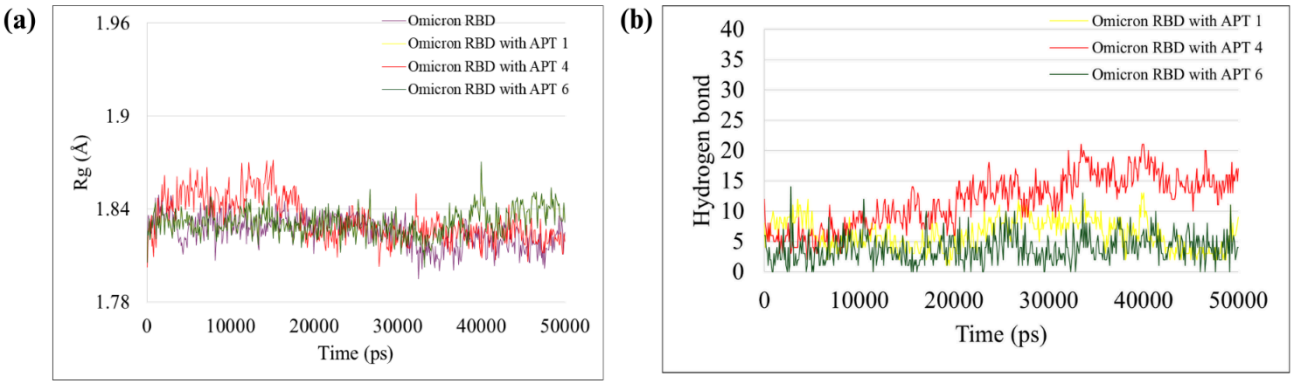

Figure 9 The Rg and Hydrogen bonding analysis of Omicron RBD and Omicron RBD-Aptamer complexes. (a) Rg of [Omicron RBD (purple), Omicron RBD-APT 1 (yellow), Omicron RBD-APT 4(red), and Omicron RBD-APT6 (green)]. (b) Hydrogen bonding of [Omicron RBD-APT 1 (yellow), Omicron RBD-APT 4(red), and Omicron RBD-APT6 (green)].

The residues of protein are essential for maintaining a stable conformation in a protein-ligand complex [21]. This stability can be assessed using the RMSF parameter. RMSF measures how much a specific segment of the protein deviates from its average structure, typically due to ligand interaction [22]. The highest fluctuations were shown by amino acids located within the loop regions of the Omicron RBD S protein and these amino acids are slightly far away from the binding site. These amino acids were found to be ASN334, TYR365, TYR369, PHE374, ASN388, LYS458, LYS478, and LYS527. Other amino acids showed lower fluctuations and maintained highest stability (Figure 8b). This indicates that these flexible loop regions experience more significant conformational fluctuations, a common characteristic since loops frequently function as dynamic elements in proteins.

Rg is used to assess the structural variations of protein during MD simulations. Rg provides insights into the protein's compactness and flexibility within a biological environment, enabling comparisons of the protein's structure over time with the experimentally measurable hydrodynamic radius [23]. All of our simulated MD systems displayed stable and consistent Rg between 1.79 Å to 1.87 Å (Figure 9a). The stable Rg values indicate that the Omicron RBD and its ligand-bound forms retain their structural integrity and compactness within the simulated biological environment. This consistency reinforces the conclusion that the protein maintains a well-folded conformation, aligning with the RMSD and RMSF analyses on system stability.

Hydrogen bonds are fundamental in nature and essential for protein folding, protein-ligand interactions, and catalysis [24]. The widespread presence and versatility of hydrogen bonds make them the most crucial physical interaction in biomolecular systems within aqueous solutions [25]. Figure 9b illustrates the number of hydrogen bonds formed between Omicron RBD and each candidate aptamer during the 50ns simulation. Omicron RBD-APT 1 shows significant fluctuations in hydrogen bond numbers, suggesting dynamic behaviour but lower stability. Omicron RBD-APT 4 exhibits the highest peak of 21 hydrogen bonds with fewer fluctuations, indicating a more stable and potentially stronger binding interaction. Omicron RBD-APT 6 is similar to Omicron RBD-APT 1 in peak values but has fewer fluctuations, suggesting some level of stability. While hydrogen bonding plays a prominent role in the strength and stability of protein-ligand interactions, it is insufficient to rely solely on this metric for a comprehensive understanding. A higher number of stable hydrogen bonds, as seen in Omicron RBD-APT 4, suggests a stronger complex. However, it is also important to consider other factors such as RMSD, RMSF, Rg and overall molecular interactions.

4.0 CONCLUSION

In conclusion, this *in silico* study evaluated multiple RNA aptamer candidates (APT 1 to APT 6) targeting the RBD of the SARS-CoV-2 Omicron variant spike protein. While all the aptamers demonstrated varying degrees of binding affinity and interaction with the RBD, APT 6 emerged as the promising candidate due to its lowest binding energy, extensive interactions with key mutated residues, and favourable stability parameters reflected in RMSD and RMSF analyses. Other aptamers, such as APT 1 through APT 5, showed moderate binding affinities and fewer interactions, indicating potential but comparatively lower effectiveness. These differences highlight the importance of detailed structural and dynamic assessments in aptamer selection.While the findings suggest promising characteristics for the selected aptamer candidate (APT 6), further validation is necessary to confirm its practical performance *in vivo*.

Acknowledgment

The authors would like to thank the Department of Biosciences, Universiti Teknologi Malaysia, for providing the necessary facilities for this research. This work was funded by the UTM PAS GRANT PY/2024/02290.

References

1. World Health Organization. (2025). *COVID-19 epidemiological update – 17 January 2025*. https://www.who.int/activities/tracking-SARS-CoV-2-variants
2. Justo Arevalo, S., Castillo-Chávez, A., Uribe Calampa, C. S., Zapata Sifuentes, D., Huallpa, C. J., Landa Bianchi, G., Garavito-Salini Casas, R., Quiñones Aguilar, M., & Pineda Chavarría, R. (2023). What do we know about the function of SARS-CoV-2 proteins? *Frontiers in Immunology, 14*. https://doi.org/10.3389/fimmu.2023.1249607
3. Huang, Y., Yang, C., Xu, X. F., Xu, W., & Liu, S. W. (2020). Structural and functional properties of SARS-CoV-2 spike protein: Potential antivirus drug development for COVID-19. *Acta Pharmacologica Sinica, 41*(9), 1141–1149. https://doi.org/10.1038/s41401-020-0485-4
4. Chen, L., He, Y., Liu, H., Shang, Y., & Guo, G. (2024). Potential immune evasion of the severe acute respiratory syndrome coronavirus 2 Omicron variants. *Frontiers in Immunology, 15*. https://doi.org/10.3389/fimmu.2024.1339660

5. Cui, Z., Liu, P., Wang, N., Wang, L., Fan, K., Zhu, Q., Wang, K., Chen, R., Feng, R., Jia, Z., Yang, M., Xu, G., Zhu, B., Fu, W., Chu, T., Feng, L., Wang, Y., Pei, X., Yang, P., … Wang, X. (2022). Structural and functional characterizations of infectivity and immune evasion of SARS-CoV-2 Omicron. *Cell, 185*(5), 860–871.e13. https://doi.org/10.1016/j.cell.2022.01.019
6. Maffei, M., Montemiglio, L. C., Vitagliano, G., Fedele, L., Sellathurai, S., Bucci, F., Compagnone, M., Chiarini, V., Exertier, C., Muzi, A., Roscilli, G., Vallone, B., & Marra, E. (2021). The nuts and bolts of SARS-CoV-2 spike receptor-binding domain heterologous expression. *Biomolecules, 11*(12). https://doi.org/10.3390/biom11121812
7. Wandtke, T., Wędrowska, E., Szczur, M., Przybylski, G., Libura, M., & Kopiński, P. (2022). Aptamers—Diagnostic and therapeutic solution in SARS-CoV-2. *International Journal of Molecular Sciences, 23*(3). https://doi.org/10.3390/ijms23031412
8. Alhamid, G., Tombuloglu, H., Rabaan, A. A., & Al-Suhaimi, E. (2022). SARS-CoV-2 detection methods: A comprehensive review. *Saudi Journal of Biological Sciences, 29*(11). https://doi.org/10.1016/j.sjbs.2022.103465
9. van Beek, J., Igloi, Z., Boelsums, T., Fanoy, E., Gotz, H., Molenkamp, R., van Kampen, J., GeurtsvanKessel, C., van der Eijk, A., van de Vijver, D., & Koopmans, M. (2020). From more testing to smart testing: Data-guided SARS-CoV-2 testing choices. *medRxiv*. https://doi.org/10.1101/2020.10.13.20211524
10. Zhou, G., Wilson, G., Hebbard, L., Duan, W., Liddle, C., George, J., & Qiao, L. (2016). Aptamers: A promising chemical antibody for cancer therapy. *Oncotarget, 7*(12). https://doi.org/10.18632/oncotarget.7178
11. Osborne, S. E., & Ellington, A. D. (1997). Nucleic acid selection and the challenge of combinatorial chemistry. In *Chemical Reviews*, *97*(2), 349–370. https://doi.org/10.1021/cr960009c
12. Dejnirattisai, W., Huo, J., Zhou, D., Zahradník, J., Supasa, P., Liu, C., Duyvesteyn, H. M. E., Ginn, H. M., Mentzer, A. J., Tuekprakhon, A., Nutalai, R., Wang, B., Dijokaite, A., Khan, S., Avinoam, O., Bahar, M., Skelly, D., Adele, S., Johnson, S. A., … Screaton, G. R. (2022). SARS-CoV-2 Omicron-B.1.1.529 leads to widespread escape from neutralizing antibody responses. *Cell, 185*(3), 467–484.e15. https://doi.org/10.1016/j.cell.2021.12.046
13. Hari, S., & Sudharsan, M. S. (2023). Molecular modeling and docking analysis of swine flu (H1N1) neuraminidase protein against the phytochemicals of *Andrographis paniculata*. *Journal of Microbiology, Biotechnology and Food Sciences, 12*(6). https://doi.org/10.55251/jmbfs.4751
14. Asif Mirza, Z., Naeem, A., Syed, A., Mateen, R. M., Fareed, M. I., & Husaain, M. (2023). In silico analysis to predict the pathogenic variants of CANT1 gene causing Desbuquios dysplasia (DBQD) type 1. *Current Trends in OMICS, 3*(1), 18–38. https://doi.org/10.32350/cto.31.02
15. Wong, F. C., Ong, J. H., & Chai, T. T. (2020). Identification of putative cell-entry-inhibitory peptides against SARS-CoV-2 from edible insects: An in silico study. *EFood, 1*(5), 357–368. https://doi.org/10.2991/efood.k.200918.002
16. Eberhardt, J., Santos-Martins, D., Tillack, A. F., & Forli, S. (2021). AutoDock Vina 1.2.0: New docking methods, expanded force field, and Python bindings. *Journal of Chemical Information and Modeling, 61*(8), 3891–3898. https://doi.org/10.1021/acs.jcim.1c00203
17. Li, Y., Liu, J., & Gumbart, J. C. (2021). Preparing membrane proteins for simulation using CHARMM-GUI. In *Methods in Molecular Biology* (Vol. 2302, pp. 237–251). Humana Press Inc. https://doi.org/10.1007/978-1-0716-1394-8_13
18. Sarkar, A., Sen, D., Sharma, A., Muttineni, R. K., & Debnath, S. (2021). Structure-based virtual screening and molecular dynamics simulation to identify potential SARS-CoV-2 spike receptor inhibitors from natural compound database. *Pharmaceutical Chemistry Journal, 55*(5), 441–453. https://doi.org/10.1007/s11094-021-02441-w
19. Bender, B. J., Gahbauer, S., Luttens, A., Lyu, J., Webb, C. M., Stein, R. M., Fink, E. A., Balius, T. E., Carlsson, J., Irwin, J. J., & Shoichet, B. K. (2021). A practical guide to large-scale docking. *Nature Protocols, 16*(10), 4799–4832. https://doi.org/10.1038/s41596-021-00597-z
20. Mulyani, D. E., Maksum, I. P., & Yusuf, M. (2024). In silico study of aptamer specificity for detection of insulin as development for diabetes mellitus diagnosis. *Indonesian Journal of Chemistry, 24*(3), 855–864. https://doi.org/10.22146/ijc.91602
21. Du, X., Li, Y., Xia, Y. L., Ai, S. M., Liang, J., Sang, P., Ji, X. L., & Liu, S. Q. (2016). Insights into protein–ligand interactions: Mechanisms, models, and methods. *International Journal of Molecular Sciences, 17*(2). https://doi.org/10.3390/ijms17020144
22. Sharma, J., Kumar Bhardwaj, V., Singh, R., Rajendran, V., Purohit, R., & Kumar, S. (2021). An in-silico evaluation of different bioactive molecules of tea for their inhibition potency against non-structural protein-15 of SARS-CoV-2. *Food Chemistry, 346*, 128933. https://doi.org/10.1016/j.foodchem.2020.128933
23. Ghahremanian, S., Rashidi, M. M., Raeisi, K., & Toghraie, D. (2022). Molecular dynamics simulation approach for discovering potential inhibitors against SARS-CoV-2: A structural review. *Journal of Molecular Liquids, 354*. https://doi.org/10.1016/j.molliq.2022.118901
24. Chen, D., Oezguen, N., Urvil, P., Ferguson, C., Dann, S. M., & Savidge, T. C. (2016). Regulation of protein-ligand binding affinity by hydrogen bond pairing. *Science Advances, 2*(3). https://doi.org/10.1126/sciadv.1501240
25. Bulusu, G., & Desiraju, G. R. (2020). Strong and weak hydrogen bonds in protein–ligand recognition. *Journal of the Indian Institute of Science, 100*(1), 31–41. https://doi.org/10.1007/s41745-019-00141-9